


Article

Study on Urea Crystallization Risk Assessment and Influencing Factors in After-Treatment System of Diesel Engines

Ke Sun ¹, Gecheng Zhang ¹ , Kui Zhao ¹, Wen Sun ¹, Guoxiang Li ¹, Shuzhan Bai ^{1,*}, Chunjin Lin ^{2,*} and Hao Cheng ³

¹ School of Energy and Power Engineering, Shandong University, Jinan 250061, China; sunkeke@sdu.edu.cn (K.S.); sdzgc@mail.sdu.edu.cn (G.Z.); 201920466@mail.sdu.edu.cn (K.Z.); sunwensdu@foxmail.com (W.S.); liguox@sdu.edu.cn (G.L.)

² Geotechnical and Structural Engineering Research Center, Shandong University, Jinan 250061, China

³ School of Aeronautic Science and Engineering, Beihang University, Beijing 100191, China; chenghao01@buaa.edu.cn

* Correspondence: baishuzhan@sdu.edu.cn (S.B.); linchunjin@sdu.edu.cn (C.L.)

Abstract: In order to meet the increasing pollutants discharge standard, the selective catalytic reduction (SCR) module in the diesel engine after-treatment system is an important means to reduce nitrogen oxide (NO_x) emissions. SCR systems are prone to urea crystallization at lower temperatures, especially during the cold-start conditions of diesel engines. In this study, we use the diesel engine after-treatment system test bench to obtain the boundary parameter of the simulation modules, and the urea crystallization risk assessment model of the diesel SCR system is established. Comparing the computational fluid dynamics (CFD) results with the test bench results, it is shown that the predicted urea film distribution of the assessment model is in good agreement with the experimental results. In order to clarify the various factors that affect the urea crystallization risk, this paper conducts a simulation analysis on a nozzle and mixer structure and operating parameters. The CFD results indicate that the increase in urea spray time will increase the maximum urea film thickness on the SCR system mixer surface. Exhaust temperature is the most important influencing factor. When the diesel engine exhaust temperature increases from 190 °C to 300 °C, the maximum urea film thickness decreases by 32 and the urea film mass accumulation decreases by 5%. Exhaust flow has a small impact on urea crystallization risk. When the exhaust flow increases from 300 kg/h to 600 kg/h, the maximum urea film thickness decreases by 39% and the urea film mass accumulation decreases by about 1%. In addition, urea spray rate, nozzle numbers, spray angle, and spray cone angle are also factors that affect urea crystallization risk.

Keywords: diesel; after-treatment; SCR; urea crystallization risk; NO_x



Citation: Sun, K.; Zhang, G.; Zhao, K.; Sun, W.; Li, G.; Bai, S.; Lin, C.; Cheng, H. Study on Urea Crystallization Risk Assessment and Influencing Factors in After-Treatment System of Diesel Engines. *Appl. Sci.* **2024**, *14*, 684. <https://doi.org/10.3390/app14020684>

Academic Editor: Jun Cong Ge

Received: 21 December 2023

Revised: 10 January 2024

Accepted: 11 January 2024

Published: 13 January 2024



Copyright: © 2024 by the authors. Licensee MDPI, Basel, Switzerland. This article is an open access article distributed under the terms and conditions of the Creative Commons Attribution (CC BY) license (<https://creativecommons.org/licenses/by/4.0/>).

1. Introduction

The diesel engine is criticized in current and future developments due to its excellent reliability and economy. The emerging energy industry currently has, more or less, problems [1–5] and cannot replace diesel engines in the short term [6]. Due to the complex composition of diesel fuel and the oxygen-rich combustion characteristics of diesel engines, the exhaust gas contains a large number of pollutants, such as carbon monoxide, nitrogen oxides (NO_x), unburned hydrocarbons (uHC), and particulate matter (PM). To control the NO_x emission level of diesel engines, selective catalytic reduction (SCR) technology is currently used in combination with an ammonia slip catalyst (ASC). In addition, to ensure the operation of a diesel oxidation catalyst (DOC) and diesel particulate filter (DPF), an SCR system is usually located downstream of an after-treatment system in accordance with emission regulations. A. A. Yusuf et al. conducted a study on the emissions of a marine diesel engine burning bio-diesel under different operating conditions. The marine

after-treatment system used in the study employs a DPF+SCR arrangement, which can effectively reduce PM and NO_x emissions levels [7,8].

At present, an SCR system generally sprays a urea water solution (UWS) into an exhaust gas. Ammonia is produced during the pyrolysis and hydrolysis processes, providing a reducing agent for NO_x catalytic conversion reactions. In ideal conditions, the droplets of UWS can completely evaporate and decompose with the help of exhaust heat. However, when the operating condition changes, the increase in ammonia demand leads to an increase in spray volume and the diameter of urea droplets. The UWS cannot be completely evaporated on the short spray path, and the droplets fall on the mixer wall to form a urea film. A thicker urea film cannot completely bring urea molecules back into the exhaust during evaporation, forming urea crystals. Henrik et al.'s research indicates that urea crystallization mainly occurs in areas such as the urea nozzle, nozzle seat, exhaust pipe wall, and the inlet surface of the carrier in the SCR system [9].

It is generally believed that urea crystal is developed from the film formed by spray hitting the wall [9,10]. The evaporation characteristics of droplets can also change at different ambient temperatures. When the ambient temperature is above 300 °C, UWS droplets will undergo deformation, hollowing, and slight explosion phenomena. By integrating the above research, the urea droplet evaporation process can be divided into two stages, namely, the water evaporates first, and then the urea begins direct pyrolysis [11]. However, some researchers also believe that water and urea are evaporated synchronously, and ammonia in the SCR system is obtained from the decomposition of urea vapor in the gas phase [12,13]. The hanging single droplet evaporation pyrolysis test can only reflect the variation process of UWS droplets in the exhaust airflow, while the crystallization process on the wall is slightly different.

If the urea spray fails to completely decompose in the exhaust, the spray may hit the wall. Spray wall impingement is a precondition for the formation of wall film, so researchers have carried out detailed research and analysis on different wall impingement behaviors. Through the spray wall impact test, Bai divided the wall impact behavior of droplets into seven types: spherical attachment, spreading attachment, complete rebound, crushing rebound, complete crushing, splash, and boiling crushing, and these seven types of behaviors are mainly divided by the Weber number of droplets and the temperature difference between the droplets and the wall surface [14]. Kuhnke further divided the region using two dimensionless numbers K and T , where the parameter K is calculated from the Weber number and Laplace number of the droplet, while T is calculated from the wall temperature and droplet saturation temperature [15].

The urea crystallization phenomenon in SCR systems is caused by a combination of factors, which can be summarized into two main categories: first, operating condition factors, such as changes in exhaust temperature, exhaust flow, and urea injection parameters; second, structural factors of the SCR system, such as mixer design and injector design.

A number of related studies have confirmed that exhaust temperature is a key factor affecting the formation of urea crystals in SCR systems. The study conducted by Navistar Corporation in the United States on urea crystallization showed that urea crystals are easily formed under low temperature and low mass flow rate conditions, with the amount of sediment generated being approximately 25~65% of the urea injection amount. When the SCR temperature reaches 350 °C, urea crystals are almost not formed [16]. Habchi et al. used a chemical reaction dynamics model to study the formation process and location of urea crystals and found that when the exhaust temperature is below the Leidenfrost temperature, a liquid film forms on the surfaces of the mixer and elbow; otherwise, after droplet collision, they leave the wall surface and tend to form a small amount of cyanuric acid in the center area of the SCR carrier inlet end surface [17].

Under actual engine operating conditions, due to the changing operating conditions, the formation characteristics of crystallization are different from those under steady-state conditions. Transient exhaust temperature, ambient temperature, and urea injection amount have different effects on the formation of crystallization [18]. Sadashiva studied the effect

of temperature changes on the total amount of crystallization by increasing the temperature of crystals generated under stable low-temperature conditions (150 °C–250 °C). The results showed that at the same injection amount, intermittent and continuous injection at low temperatures (150 °C) had a small impact on the total amount of crystallization, but intermittent temperature rise could eliminate the crystals generated during the period of no injection, thereby reducing the total amount of crystallization [19]. Overall, crystallization is greatly affected by exhaust temperature. For both steady-state and transient operating conditions, increasing temperature will improve the crystallization.

The spray parameters also have a significant impact on crystallization. The spray state can be described by spray cone angle, penetration distance, and spray particle size and distribution. The spray particle size and penetration distance are directly affected by the spray pressure. With the increase of spray pressure, the penetration distance will become larger while the spray particle size decreases. Spray particle size is generally characterized by Sauter Mean Diameter (SMD) [20]. Smaller particle size has a larger specific surface area, which is conducive to UWS evaporation and decomposition. At the same time, smaller particles are more susceptible to the influence of airflow, and the mixing effect with the exhaust is better, which improves the uniformity of ammonia distribution in the exhaust [21,22].

The formation of urea crystals can have many adverse effects: crystallization reduces the flow cross-sectional area of the carrier and increases the backpressure of the after-treatment system, which is detrimental to the fuel economy of the engine; crystallization means that some UWS is not decomposed to produce ammonia, resulting in insufficient supply of ammonia to the SCR system, which leads to a decrease in NO_x conversion efficiency. At the same time, partial decomposition of the crystallization under high-temperature conditions may lead to an excessive supply of ammonia and excessive escape of ammonia; as the crystallization problem continues to worsen, the after-treatment system may fail due to clogging, further affecting the NO_x conversion efficiency.

This article studies the urea crystallization risk assessment model for the SCR system. Through a three-dimensional simulation model, a crystallization risk assessment is conducted. Various factors affecting the crystallization process of diesel SCR systems, such as exhaust temperature, mass flow rate, spray parameters, and mixer structural parameters, are studied, and the formation process of crystallization risks is analyzed.

2. Urea Crystallization Risk Assessment Method and Simulation Model Construction

2.1. Risk Assessment Method for Urea Crystallization

In order to comprehensively evaluate the risk of urea crystallization, evaluation indicators were defined for the risk of urea crystallization. The more urea film is generated inside the SCR system, the greater the impact on the performance of after-treatment denitrification (DeNO_x) and the higher the crystallization risk. The product of the local density of the urea film and the local thickness of the urea film are defined as the local surface mass density of the urea film. By integrating the mass density in the urea film region, the cumulative amount of urea film mass m_{cum} can be obtained as follows:

$$m_{cum} = \int m_f da = \sum h_f \rho_f A_f, \quad (1)$$

where h_f is the thickness of the liquid film, ρ_f is the density of the liquid film, A_f is the surface area of the unit.

Similarly, the cumulative amount of each component i in the liquid membrane is as follows:

$$m_{cum_i} = \sum h_f \rho_f Y_i A_f, \quad (2)$$

where Y_i is the local mass fraction of component i .

The urea consumption rate is defined as the ratio of the accumulated amount of urea in the urea film to the theoretical accumulated amount of urea entering the exhaust pipe, as follows:

$$l_{urea} = \frac{m_{cum}}{0.325m_{UWS}}. \quad (3)$$

It can reflect the extent of urea consumption caused by the formation of urea film in the SCR system.

In this article, the maximum urea film thickness index will also be used as one of the evaluation indicators for urea crystallization risk in the SCR system.

2.2. Urea Crystallization Risk Prediction and Assessment Model

To realize the crystallization risk prediction of a diesel engine SCR system by means of three-dimensional numerical simulation, it is significant to comprehensively consider the relevant physicochemical processes inside the system, mainly including gas flow, heat transfer, spray atomization, component evaporation, spray wall interaction, urea film formation, and urea decomposition reaction. This chapter analyzes the relevant processes of the SCR system and establishes physical models to describe each process in sequence. A CFD model containing a Lagrangian discrete phase was established and coupled with a urea thermal decomposition reaction kinetics model containing 12 steps to achieve a numerical prediction of the crystallization risk in a diesel engine SCR system. To ensure the feasibility of the model, a comprehensive validation was conducted on the established physical model.

2.2.1. Flow and Heat Transfer Model

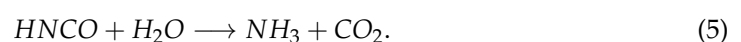
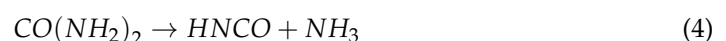
The flow model uses the time-averaged mass equation and Navier Stokes equation, while the turbulent phase is modeled using the standard equation. A two-layer fully mixed wall function is used to model the boundary layer region, and the turbulent energy dissipation rate on the centroid of the first grid layer near the wall is directly specified. Establish a gas-solid two-phase coupled heat transfer model within the SCR system, taking into account the thermal response of SCR system components.

2.2.2. Atomization, Evaporation, Multi-Interaction, and Liquid Film Model

Based on the Lagrangian method, the motion of UWS droplet particles in the flow field is described, and the Rosin Rammler method is used to define the initial droplet size distribution. Use a multi-component evaporation model to describe the evaporation of urea droplets. Establish the interaction between urea atomization droplets, exhaust pipes, and mixer walls using a well validated Bai Gosman model. Assuming the urea film is in a laminar flow state, the control equation of the urea film is discretized in the three-dimensional shell region, and a urea film model is established.

2.2.3. Chemical Reaction Kinetics Model

The ideal urea thermal decomposition reaction path includes a two-step turnkey reaction, and the reaction equations are shown as follows:



Schaber et al. [17] proposed a more detailed chemical reaction path, which includes 15 steps of chemical reactions involving urea and its thermal decomposition product (biuret, cyanuric acid, cyanuric acid monoamide, cyanuric acid diamine, and melamine). This article reasonably simplifies the chemical reaction path proposed in the literature, ignoring reaction products with extremely low yields, such as ammonium cyanurate and melamine. The simplified chemical reaction path is shown in Table 1, which includes 12 steps of

chemical reactions, including the gas phase reaction (R1,R2), urea film reaction (R3), and interphase reaction (R4~R12).

Table 1. Reaction and rate parameters related to urea pyrolysis.

Code	Chemical Reaction	A	$E_a (\times 10^4 \text{ J/mol})$	Source
R1	$\text{Urea}(g) \rightarrow \text{HNCO}(g) + \text{NH}_3(g)$	4.900×10^3	2.3	[23]
R2	$\text{HNCO}(g) + \text{H}_2\text{O}(g) \rightarrow \text{NH}_3(g) + \text{CO}_2(g)$	2.500×10^5	6.22	[23]
R3	$\text{Urea}(m) + \text{HNCO}(l) \rightarrow \text{Biuret}(m)$	3.517×10^{11}	7.545	[24]
R4	$\text{Urea}(m) \rightarrow \text{HNCO}(l) + \text{NH}_3(g)$	2.000×10^4	7.4	[24]
R5	$\text{Biuret}(m) + \text{HNCO}(g) \rightarrow \text{Cya}(s) + \text{NH}_3(g)$	9.397×10^{20}	15.868	[24]
R6	$2\text{Biuret}(m) \rightarrow \text{Cya}(s) + \text{HNCO}(g) + 2\text{NH}_3(g)$	2.327×10^{24}	38.155	[25]
R7	$\text{Biuret}(s) + \text{HNCO}(g) \rightarrow \text{Ammelide}(s) + \text{H}_2\text{O}(g)$	5.244×10^{18}	24.85	[25]
R8	$\text{Cya}(s) + \text{NH}_3(g) \rightarrow \text{Ammelide}(s) + \text{H}_2\text{O}(g)$	7.013×10^{20}	29.665	[26]
R9	$2\text{Biuret}(m) \rightarrow \text{Ammelide}(s) + \text{HNCO}(g) + \text{NH}_3(g) + \text{H}_2\text{O}(g)$	2.327×10^{26}	25.776	[24]
R10	$\text{Ammelide}(s) + \text{NH}_3(g) \rightarrow \text{Ammeline}(s) + \text{H}_2\text{O}(g)$	2.518×10^{21}	31.063	[26]
R11	$\text{Biuret}(m) \rightarrow \text{Urea}(m) + \text{HNCO}(l)$	1.107×10^{21}	20.823	[24]
R12	$\text{Cya}(s) \rightarrow 3\text{HNCO}(g)$	1.001×10^3	11.842	[24]

$\text{Urea} = \text{CO}(\text{NH}_2)_2$, $\text{Biuret} = \text{C}_2\text{H}_5\text{N}_3\text{O}_2$, $\text{Cya} = \text{C}_3\text{H}_3\text{N}_3\text{O}_3$, $\text{Ammelide} = \text{C}_3\text{H}_4\text{N}_4\text{O}_2$, $\text{Ammeline} = \text{C}_3\text{H}_5\text{N}_5\text{O}$.

3. Experiments

3.1. Simulation Model Input Conditions

The structure of the after-treatment system is shown in Figure 1, and the integrated after-treatment system adopts the technical route of DOC+DPF+SCR+ASC. Among them, the SCR system mainly consists of an injector, a mixing section, and an SCR carrier. The U-shaped after-treatment and tightly coupled layout can enhance the utilization of vehicle space and reduce the heat loss of exhaust. The static mixer is of the swirl plate type, consisting of a rotating stream tray and a porous tube, arranged coaxially to promote the mixing effect of the airflow, and improving the evaporation decomposition and uniform mixing of UWS.

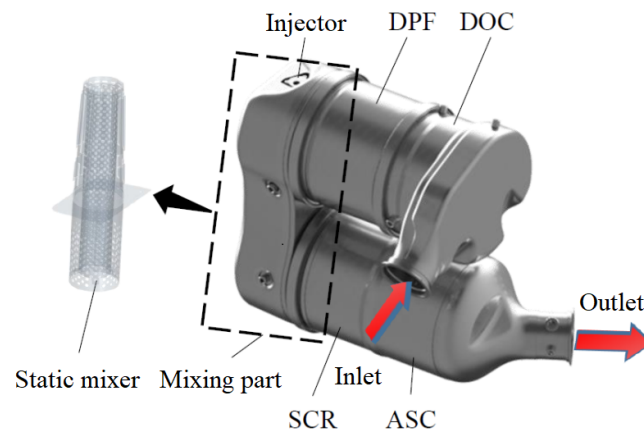


Figure 1. After-treatment system diagram.

The injector model is a 3-hole Bosch high-flow nozzle with a nozzle diameter of 190 μm . The diameter of the circle where the spray hole is located is 1.9 mm. The spray pressure is maintained at 7 bar (relative pressure), and the spray frequency is 1 Hz. The spray rate is adjusted by controlling the duty cycle. Fitting the particle size distribution using the Rosin Rammler method resulted in a particle reference diameter of 85 μm . The uniformity index of the particle size distribution is 3.3154.

The computational domain includes carriers of SCR and ASC, both of which have a straight-through structure and consistent structural parameters. The relevant parameters are shown in Table 2.

Table 2. Carrier structure parameters.

Parameter	Value
Carrier diameter	12 in
Carrier length	6 in
Carrier pore density	400 cpsi
Wall thickness	4 mil

The pore structure of the carrier has the characteristic of being narrow and long, and the number of pores is numerous, making it impossible to establish a detailed three-dimensional model for calculation. Therefore, the resistance characteristics of the carrier are added to the calculation model by adding source terms to the momentum equation. The viscosity term and the inertia term are two parts of the momentum source term, and the calculation formula for the resistance in the carrier region is as follows:

$$f = -(P_v + P_i|v_s|) \cdot v_s, \quad (6)$$

where P_v is the viscous resistance coefficient tensor, P_i is the inertial resistance coefficient tensor, v_s is the surface flow velocity. According to the pressure drop curve of the carrier, the viscous resistance coefficient and inertial resistance coefficient were fitted, and the viscous resistance coefficient values were $1520 \text{ kg} \cdot \text{m}^{-3} \cdot \text{s}^{-1}$ and $2.32 \text{ kg} \cdot \text{m}^{-4}$, respectively.

Based on the adaptive polyhedral mesh and boundary layer mesh generation strategy, the entire computational domain is discretized spatially and divided into two parts: the fluid domain and the solid domain. The basic size of the global mesh is 0.01 m, and the minimum can reach 2 mm. In the fluid domain, polyhedral grids are used, and two layers of boundary layers are set up. The total thickness of the boundary layer mesh is 2.1 mm, with a growth rate of 1.2. Since the minimum mesh size can reach 1/5 of the basic size, the fluid domain mesh is refined in the region near the wall surface, and the refined mesh region plays a certain role in the boundary layer. For the purpose of reducing computational resources, the number of layers of the boundary layer is set to 2. The solid area belongs to a thin-walled structure and is divided into two layers of thin body meshes. The relevant parameters are shown in Table 3.

Table 3. Simulation model mesh parameters.

Domain	Parameter	Value
Global	Base mesh size	0.01 m
	Min mesh size	0.002 m
Solid Domain	thin mesh layer number	2
	mesh size	0.005 m
Fluid Domain	Boundary layer number	2
	Total thickness of boundary layer mesh	0.0021 m
	Growth rate	1.2

In order to achieve a common node between two computational domain meshes at the interface, the solid domain mesh generation is first completed, and then the fluid domain mesh generation is carried out. The details of the computational domain and some mesh models are shown in Figure 2.

To ensure that the simulation calculation results have a low correlation with the mesh, the pressure drop of the SCR system is selected as the verification indicator for mesh independence. Keeping the boundary layer mesh parameters unchanged, by adjusting the basic size of the mesh, 10 mm, 8 mm, and 6 mm were obtained, with a number of meshes of 3 million, 4 million, and 5 million, respectively. The pressure drop calculation results are shown in Figure 3, and it can be proved that the pressure drop is no longer related to the

number of meshes. Compared to the test results of 7.81 kPa, the maximum error does not exceed 8%.

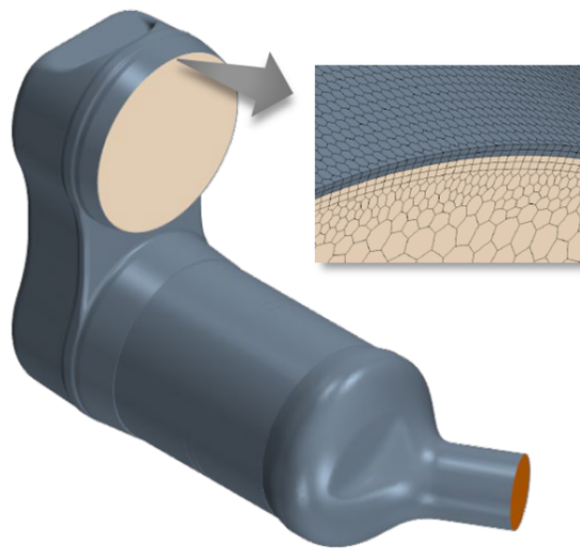


Figure 2. Mesh model diagram.

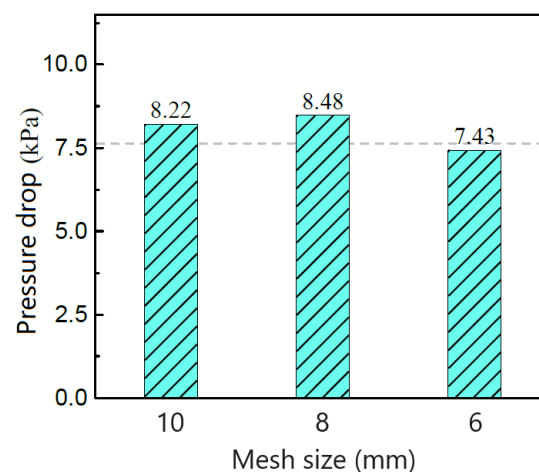


Figure 3. Mesh independence verification.

3.2. Simulation Results and Experimental Verification

From an energy perspective, it can be considered that the risk of crystallization is the result of a game between the available heat in the exhaust and the heat required for the complete evaporation and decomposition of UWS. At a certain exhaust temperature, the size of the urea spray rate determines the crystallization situation. This section selected a set of typical operating conditions at low exhaust temperature and a set of rated operating conditions at high exhaust temperature to testify to the reliability of the model and characterize the SCR system's ability to resist crystallization risks under all operating conditions. The operating parameters are listed in Table 4.

Table 4. Selected operating condition parameters.

Parameter	Rated Condition	Typical Condition
Exhaust temperature/°C	539	225
Exhaust flow rate/kg/h	1384.8	218.2
Injection rate/mg/s	1385.5	47.0
Ambient temperature/°C	25	25

The thickness and distribution of the urea film 10 ms after spraying of the injector (ASOI) are shown in Figure 4. It can be seen that a urea film is formed on the inner wall of the porous tube and the pore wall of the porous tube, with an overall macroscopic morphology similar to a “spiral band”, and no urea film is produced in other parts. The maximum local urea film thickness is 6.92×10^{-6} m, appearing closer to the injector, with a common urea film thickness of about 1×10^{-6} m in other areas. As the spray distance increases, the maximum urea film thickness gradually decreases.

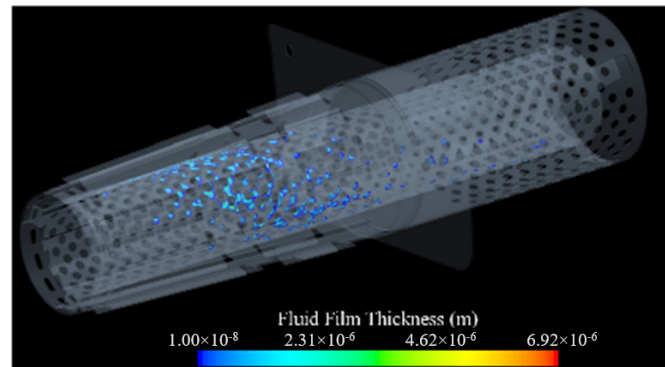


Figure 4. Urea film thickness and distribution ($t = 10$ ms ASOI).

The droplets of urea aqueous solution collide with the wall and transform into a urea film; thus, the distribution of the urea film is related to the evolution process of the droplets. The distribution results of spray particles are displayed in Figure 5. The droplets did not form a uniform spatial distribution after leaving the injector, and the UWS droplets sprayed into the exhaust from each orifice do not penetrate forward along the axis of the single spray beam but have a significant deflection. Non-colliding droplets continue to move along the spiral trajectory; they continue to interact with the rear wall surface and form a urea film under the action of centrifugal force. Finally, a “spiral ribbon” macroscopic form of the urea film is formed.

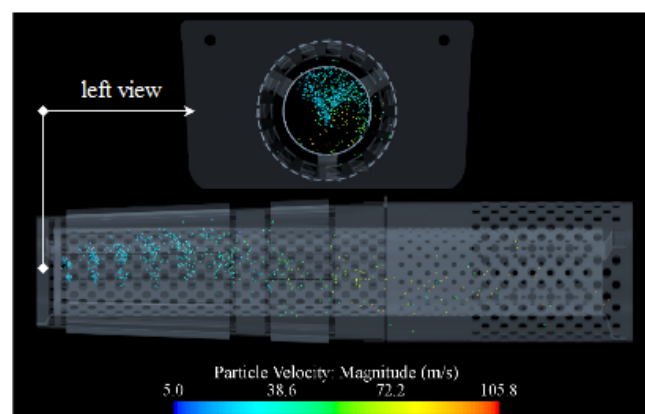


Figure 5. Spatial distribution of droplets in UWS atomization.

The flow state of exhaust gas can significantly affect the movement process of urea droplets. To clarify the influence of the exhaust flow field on droplet distribution, the distribution results of exhaust flow lines inside the mixing section of the SCR system are shown in Figure 6. The uniform airflow undergoes a significant change in its motion state after entering the SCR mixer. The left view shows the exhaust flow state inside the porous tube. It can be seen that there is a regular vortex distribution inside the porous tube, and the closer it is to the vortex center, the greater the airflow velocity, reaching a maximum of 127.4 m/s.

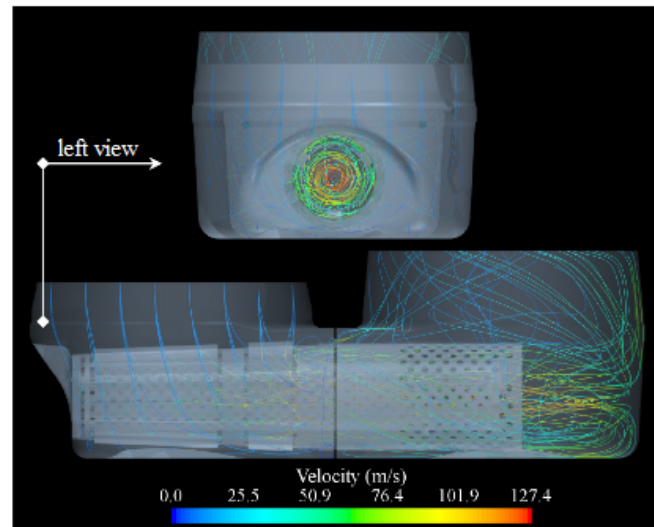


Figure 6. Flow line distribution in the mixing section of the SCR system.

The mass accumulation of urea and urea film over time is shown in Figure 7. It can be seen that at 4 ms ASOI, a urea film begins to form, and the mass accumulation of the urea and urea film increases linearly with time. Due to the continuous spray of UWS into the exhaust pipe at a certain rate, the total mass of the urea film will continue to increase at a certain rate. When the evaporation rate of urea film components is much lower than the mass replenishment rate of the urea film, the total mass of the urea film shows an almost linear increase trend. From the variation curve of the urea loss rate in the figure, it can be seen that the SCR system has caused considerable urea loss due to the formation of a urea film. The urea loss rate shows a continuously increasing trend. After starting the spray, it first increases at a faster rate to around 4.5% and then slows down. At 50 ms ASOI, the urea quality loss rate reached 5.6%, but at this point, the urea loss rate has not yet reached stability, indicating that the urea loss rate will continue to increase with the spray process until it stabilizes.

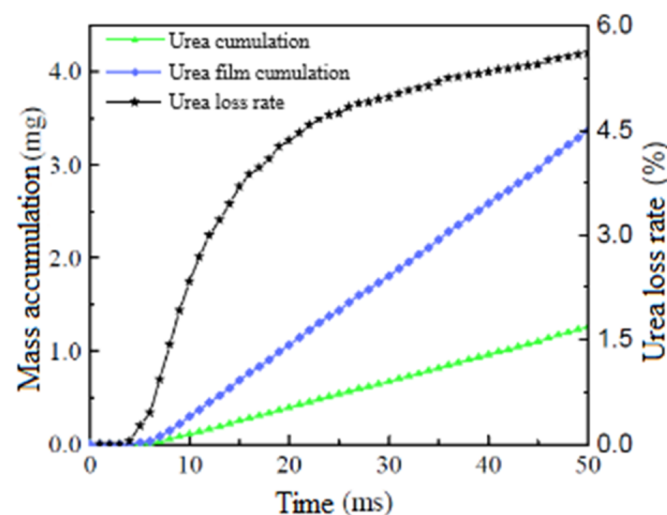


Figure 7. Accumulation of urea and urea film mass and changes in urea loss rate over time.

The crystallization situation inside the SCR system mixer in the experiment is compared with the area where the urea film appears in the simulation in Figure 8. A considerable amount of urea crystals have formed on the inner wall of the porous tube. At a location closer to the injector, the crystals exhibit a “spiral band” distribution. At a distance from the injector, there is a relatively small amount of urea crystals present, exhibiting a “dot

like” distribution. UWS forms a urea film on the inner wall of the mixing tube. Due to the accumulation rate of the urea film being lower than the consumption rate, the urea film continues to accumulate and gradually solidifies into crystals in a low exhaust temperature environment. At the location near the injector, the eddy current has not yet fully developed, resulting in a weaker blowing effect of the airflow, forming a “spiral strip” distribution of crystals. With the development of an eddy current, the blowing effect of the airflow in the rear section of the mixing tube is strengthened, and in addition, UWS droplets are relatively dispersed, ultimately forming a “dot-like” distribution of crystals. Compared with the simulation results in the previous section, the distribution position of crystals is basically consistent with the formation position of urea film, and there is also a similarity in the distribution morphology, indicating that the crystallization risk prediction method used in this chapter for the SCR system of diesel engines is reasonable.

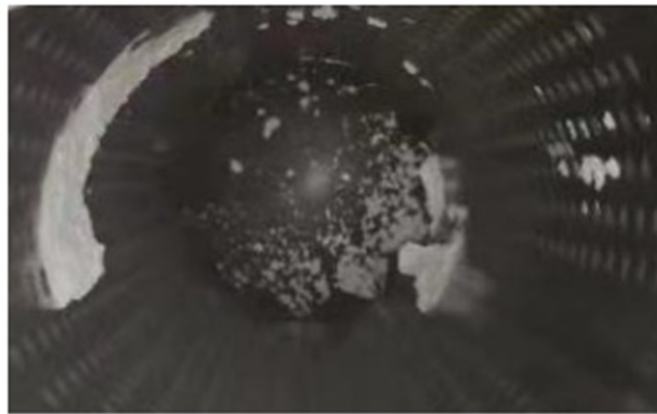


Figure 8. Comparison of urea crystallization and simulation results.

4. Results

4.1. Influence of Urea Crystallization Risk under Operating Conditions

4.1.1. Research Protocol

In order to ensure the representativeness and guidance of the research on the factors affecting crystallization risk, while also considering the calculation cost, special attention has been paid to specific operating conditions. Considering that the crystallization phenomenon mainly occurs in low to medium temperature conditions with low exhaust temperature, and the starting temperature of urea solution is 190 °C, the exhaust temperature range is selected as 190~300 °C. Based on the actual range of exhaust flow rate in the mixing section of the SCR system of the diesel engine in use, the exhaust flow rate range is selected as 60~500 kg/h.

By adopting the method of controlling factors, the multi-factor problem is simplified into a single-factor problem, and a set of benchmark operating conditions are set, namely, exhaust temperature of 240 °C, the exhaust flow rate of 300 kg/h, urea spray rate of 0.24 g/s, number of spray holes of 3, single hole spray angle of 30°, single fog beam cone angle of 15°, and swirl plate angle of 30°. When studying a certain factor, only the parameter of that factor is considered as the unique variable, and other parameters are used as benchmark operating conditions parameters.

4.1.2. Influence of Exhaust Temperature on Urea Crystallization Risk

The variation of maximum urea film thickness with time at different exhaust temperatures is in Figure 9. The maximum urea film thickness gradually increased with the extension of spray time. At 200 ms ASOI, the maximum urea film thickness is already in the thickness range of 300~500 µm. After turning on the UWS spray, the atomized UWS droplets enter the exhaust at a faster speed. Subsequently, a portion of the droplets collide with the wall of the porous tube and interact with it, forming a urea film on the mixing tube. The urea film continues to develop and accumulate as the spray continues, resulting in the

maximum urea film thickness continuously increasing with the extension of spray time. Before the ASOI time of 100 ms, there was inapparent difference in the maximum urea film thickness at different temperatures; however, after the ASOI time of 100 ms, the difference in maximum urea film thickness at different temperatures is significant, and the difference is stable, indicating that the comparison of crystallization risk difference needs to be based on the results of stable urea film development trend.

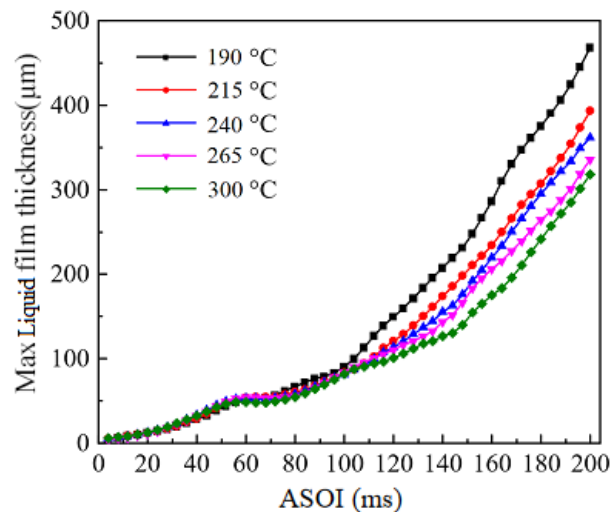


Figure 9. Variations of maximum urea film thickness with time under different exhaust temperatures.

Extract urea film mass accumulation data at different exhaust temperatures at 200 ms ASOI time, and obtain the variation of urea and UWS film mass accumulation with the exhaust temperature, as shown in Figure 10. The accumulation of urea film decreased with the increase in exhaust temperature, indicating that an increase in exhaust temperature is beneficial for reducing the urea film. The exhaust temperature increased from 190 °C to 300 °C, and the accumulation of urea film decreased by about 5%. In the temperature range exceeding 240 °C, the impact of temperature increase on the accumulation of urea film mass was more significant, indicating that the increase in exhaust temperature has a better inhibitory effect on crystallization risk.

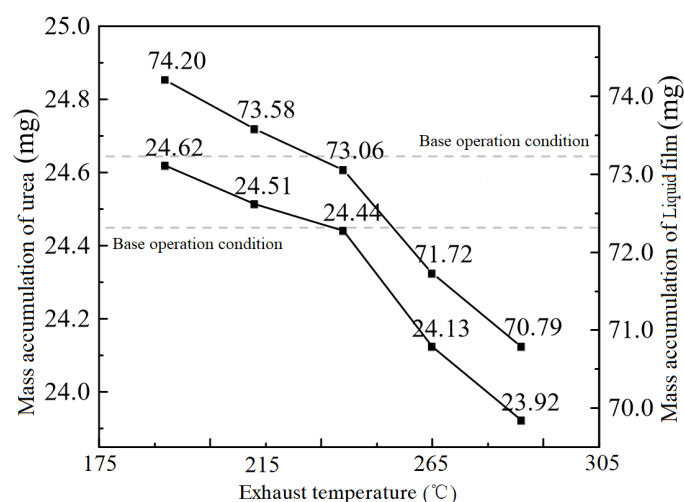


Figure 10. Variations of urea and UWS film mass accumulation with exhaust temperature.

4.1.3. Influence of Exhaust Flow Rate on Urea Crystallization Risk

The variation of maximum urea film thickness with time under different exhaust flow rates is shown in Figure 11. The maximum urea film thickness under each exhaust flow

rate gradually increases with the extension of spray time. At the time of 200 ms ASOI, the maximum urea film thickness is already in the thickness range of 200~500 μm . The growth of the maximum urea film thickness under different operating conditions shows a “two-stage” growth trend. In the front and back intervals of the turning point between the two stages, the growth trend of the maximum urea film thickness is different. It indicates that the formation of urea film undergoes two stages: initial urea film formation and continuous accumulation of urea film. In the first stage, there is a small difference in the maximum urea film thickness under various operating conditions, while in the second stage, there is a significant difference.

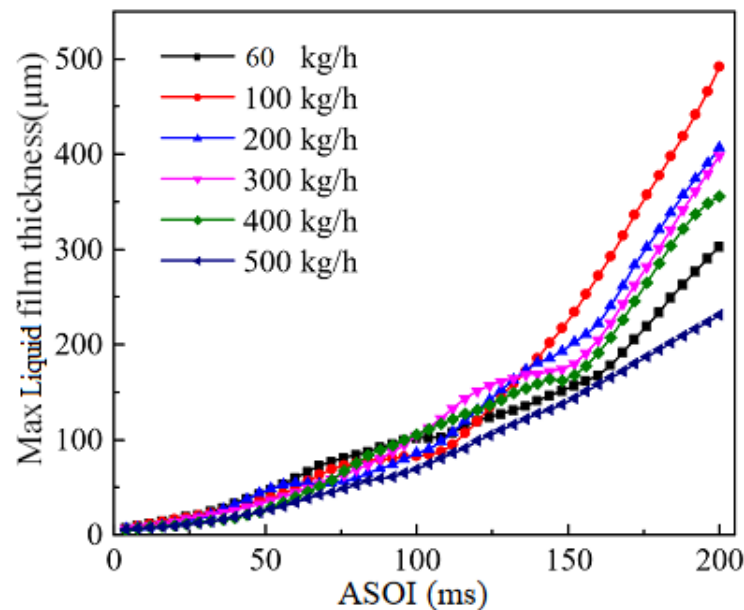


Figure 11. The variation of maximum urea film thickness with time under different exhaust flow rates.

Extract the maximum urea film thickness data under different exhaust flow rates at 200 ms ASOI time, and obtain the variation of the maximum urea and UWS film thickness with the exhaust flow rate in Figure 12. The variation trend of the maximum urea and UWS film thickness under low flow conditions is consistent with that under high flow conditions. In the range of 60 kg/h to 200 kg/h, the maximum urea film thickness increased first and then decreased with the increase of exhaust flow rate. In the range of 200 kg/h to 500 kg/h, the trend is also the same, with the difference being that the latter has a smaller amplitude of change than the former. In the urea SCR mixing section, different exhaust flow rates will form different flow field distributions, thereby affecting the spatial distribution and evolution process of UWS droplets. Under low exhaust flow conditions, the flow field distribution promotes the concentrated wall collision behavior of UWS droplets. Under high exhaust flow conditions, the flow field distribution promotes the dispersion of droplet particles in space and reduces the amount of concentrated wall collision in UWS, thereby inhibiting the accumulation of urea film concentration and reducing the risk of crystallization.

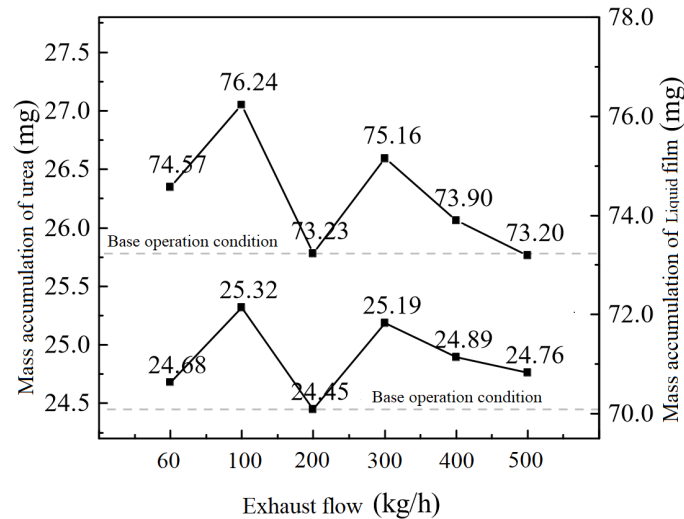


Figure 12. Variations of urea and UWS film mass accumulation with exhaust flow rates.

4.1.4. Influence of the Urea Spray Rate on Crystallization Risk

The variation of maximum urea film thickness with time under different UWS spray rates is shown in Figure 13. The trend of maximum urea film thickness variation under different UWS spray rates is basically consistent and gradually increases with the extension of spray time. At 200 ms ASOI, the maximum urea film thickness at different UWS spray rates has already been between 150~650 μm . At a high spray rate of 0.32 g/s, the growth trend is most obvious. However, at a low spray rate of 0.16 g/s, the turning point of the stage is not clear. In the interval before the 75 ms ASOI time, there is a small difference in the maximum urea film thickness under each working condition. After the 150 ms ASOI time, there is a difference in the maximum urea film thickness under each working condition. This difference indicates that the UWS spray rate can have a significant impact on crystallization risk.

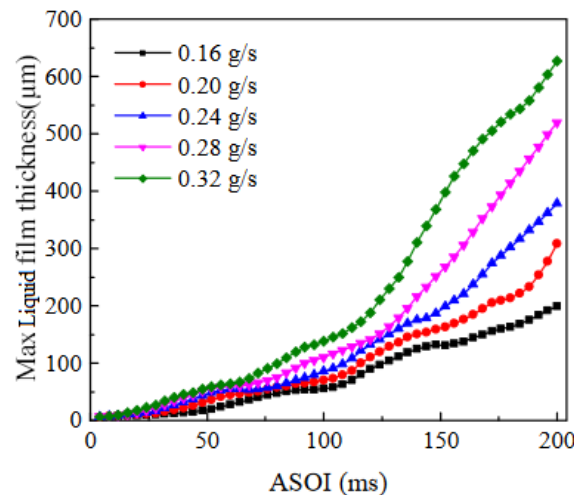


Figure 13. Variations of maximum urea film thickness with time under different UWS spray rates.

Extract the urea film mass accumulation data under different UWS spray rates at 200 ms ASOI time, shown in Figure 14. The accumulation of urea film mass increases with the UWS spray rate and shows a positive correlation. Taking the benchmark operating conditions as a reference, an increase of 0.8 g/s in spray rate results in a 27% increase in urea film accumulation. On the contrary, a decrease of 0.8 g/s in spray rate results in a 30% decrease in urea film accumulation, indicating that the UWS spray rate can significantly affect urea film accumulation. Based on the impact of the UWS spray rate on the maximum

urea film thickness, the UWS spray rate has a significant impact on the crystallization risk of the system. When formulating the spray control strategy for the urea SCR system, it is important to minimize the UWS spray rate as much as possible to reduce the crystallization risk of the system.

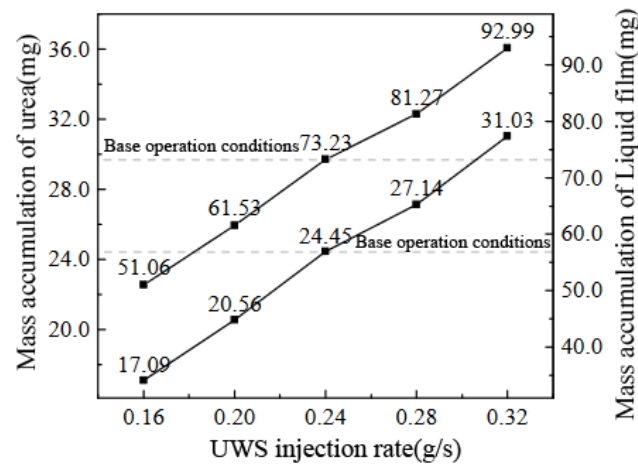


Figure 14. Variations of urea and UWS film mass accumulation with urea spray rate.

4.1.5. Influence of Urea Film Consumption Rate

Figure 15 shows the urea film retention ratio at different exhaust temperatures. The urea film retention ratio changes with temperature. As the temperature increases, the overall trend of the urea film retention ratio increases first and then decreases. When the temperature reaches 220 °C, the urea film retention ratio reaches 0.324%. When the temperature is greater than 220 °C, the urea film retention ratio begins to decrease, dropping to 0.314% at 380 °C, which is 0.01% lower than the urea film retention ratio at 220 °C. As the temperature increases, the activity of urea surface molecules increases, thereby accelerating the rate of urea molecule evaporation from the urea surface. Therefore, as the temperature increases, the thickness of the urea film gradually decreases, showing a decrease in the retention ratio of the existing urea film.

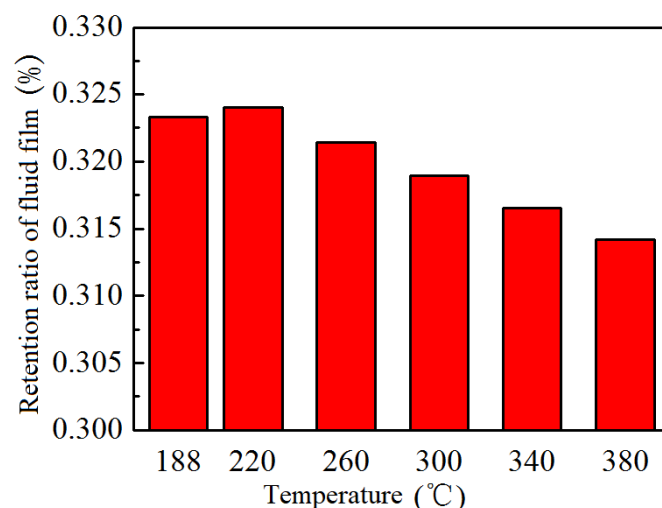


Figure 15. The trend of urea film retention ratio changing with temperature.

Figure 16 shows the trend of urea film retention ratio with different flow rates. When the flow rate is 428 kg/h, the urea film retention ratio is 0.323%. As the flow rate increases, the urea film retention ratio gradually decreases. When the flow rate is

628 kg/h, the urea film retention ratio decreased to the lowest, at 0.308%. The retention of urea film decreased by 4.64% compared to a flow rate of 428 kg/h. The exhaust flow rate factor can simultaneously affect the total wall collision amount of urea aqueous solution. Under different exhaust flow rates, there were significant differences in the internal film distribution of the SCR system, further affecting the motion trajectory of urea aqueous solution atomized droplets in the airflow. Droplets with larger particle sizes have greater inertia and are less affected by airflow, while droplets with smaller particle sizes have less inertia and may experience trajectory deflection under the influence of airflow, thereby avoiding droplet wall collision and reducing the amount of droplet wall collision.

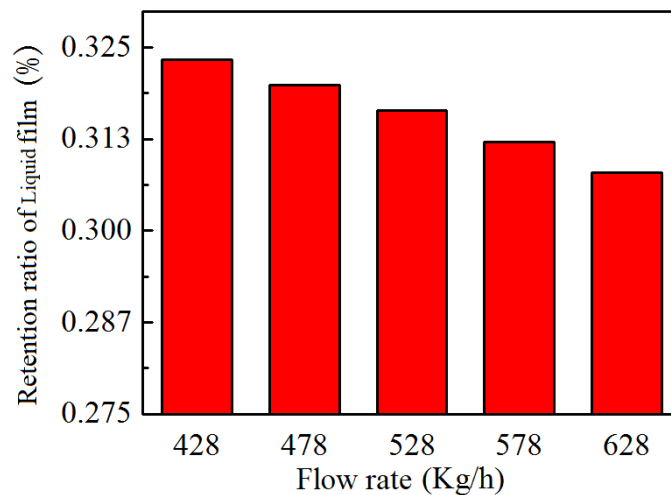


Figure 16. The trend of urea film retention ratio changing with flow rate.

The trend of urea film accumulation over time is displayed in Figure 17. With the increase of time, the accumulation of urea film also increases. Specifically, within the time period of 0~1 s, the accumulated amount of urea film shows a linear growth trend because the spray rate of urea is relatively high during this time period. During the period of 1~3 s, the accumulation of urea film still showed a linear increase trend, but the growth rate decreased compared to the previous period due to a decrease in the urea solution spray rate during that period. Near 3 s later, the accumulation of urea film reached its peak and slightly decreased due to a decrease in the urea spray rate of the SCR system at that time. Overall, there is a correlation between the variation of urea film accumulation over time and the variation of urea solution spray rate over time.

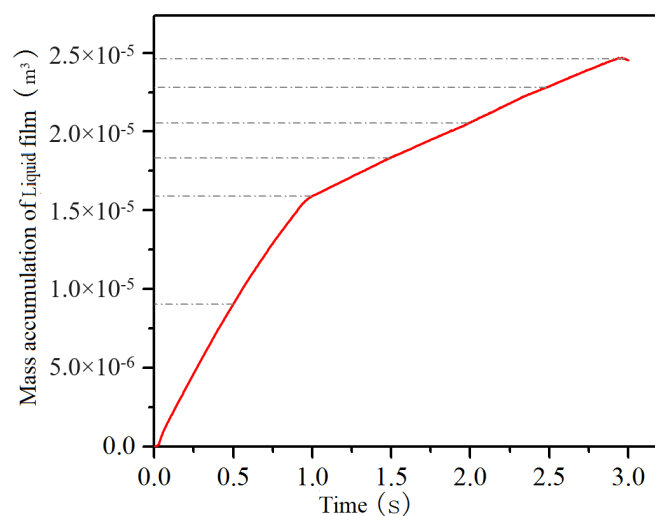


Figure 17. The trend of urea film accumulation over time.

Figure 18 shows the trend of urea film retention ratio over time from 0 to 3 s. During the time period of 0~0.2 s, the urea film retention ratio rapidly increases. Within 0.2~0.4 s, the urea film retention ratio reaches its peak and begins to stabilize. At this point, the urea film retention ratio approaches 0.6%. Subsequently, within 0.4~3 s, the urea film retention ratio gradually decreases with time, and at 3 s, the urea film retention ratio is 0.37%. Comparing the changes in urea film accumulation over time within 0~3 s, it can be found that there is no positive correlation between the urea film retention ratio and the urea film accumulation. That is, as the spraying continues, the urea film accumulation gradually increases, while the urea film retention ratio gradually decreases after the formation of the urea film.

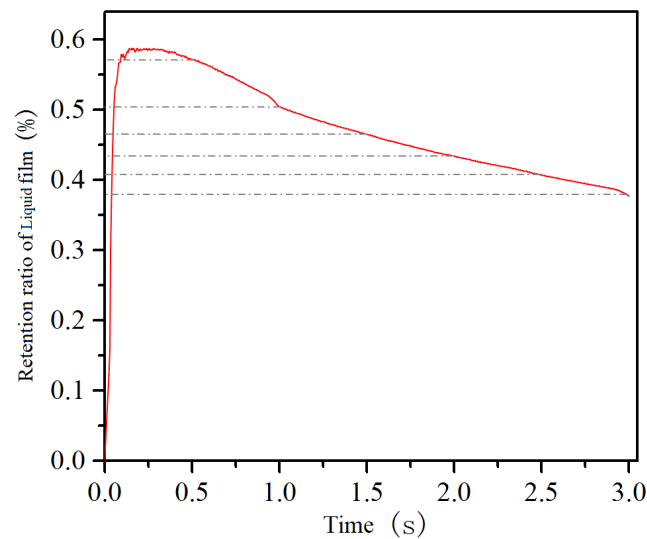


Figure 18. The trend of retention ratio of urea film over time (0~3 s).

Figure 19 shows the trend of liquid film retention ratio over time within 1~6 s. From the graph, it can be seen that within the 1~6 s time period, as time increases, the liquid film retention ratio shows a decreasing trend, and the rate of decline gradually decreases. At 6 s, the liquid film retention ratio was 0.28%, reaching the lowest value throughout the entire time period. Before 3 s, the injection continued, causing the liquid film to gradually accumulate. At the same time, due to the decrease in injection rate, the retention ratio of the liquid film gradually decreased. At 3 s, the urea solution injection was stopped, and as the remaining liquid film continued to evaporate, the retention ratio further decreased.

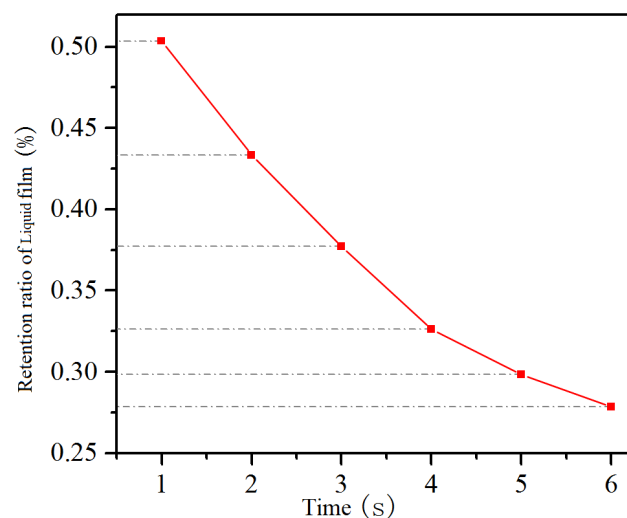


Figure 19. The trend of urea film retention ratio over time (1~6 s).

4.2. Influence of Urea Crystallization Risk under Structural Factors

The parameters that this section focuses on include rotating-stream tray, number of spray holes, single-hole spray angle, and single mist beam cone angle. By exploring the impact of these four key parameters on crystallization risk, guidance is provided for the formulation of spray strategy and injector selection in SCR systems.

4.2.1. Influence of the Rotating-Stream Tray Angle on Crystallization Risk

The spray parameters have a direct correlation with the performance of atomization evaporation, which in turn affects the crystallization risk. The structural characteristics of the SCR mixer impact fluid dynamics, further affecting the spatial distribution and crystallization risk of UWS atomized droplets. In order to clarify the influence of the rotating-stream tray on the crystallization risk of the mixer, three different layouts of rotating-stream tray angles were selected in Figure 20.

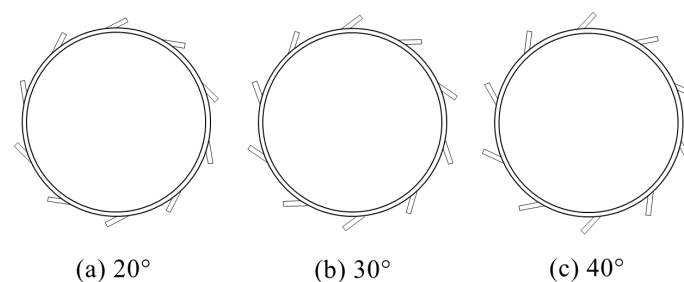


Figure 20. Three types of rotating-stream tray angles layout.

The variation of the maximum urea film thickness with time under different rotating-stream tray angles is displayed in Figure 21. The maximum urea film thickness under different rotating-stream tray angles gradually increases with the extension of spray time, and the difference in the maximum urea film thickness value is small. At the time of 200 ms ASOI, the maximum urea film thickness corresponding to each rotating-stream tray angle is only in the thickness range of 340~400 μm , indicating that the rotating-stream tray angle has a certain impact on the maximum urea film thickness, but this effect is smaller than other factors. Before the ASOI time of 100 ms, the maximum urea film thickness under the three different rotating-stream tray angle layouts is basically the same. After the ASOI time exceeds 100 ms, the maximum urea film thickness corresponding to a rotating-stream tray angle of 20° is always slightly lower than the corresponding values of the other two angles. In the ASOI range of 100~160 ms, the maximum urea film thickness corresponding to a rotating-stream tray angle of 40° is slightly higher than the other two angles. Overall, the development process of the maximum urea film thickness is less impacted by the layout of different rotating-stream tray angles.

Extract urea and UWS film mass accumulation data at different rotating-stream tray angles at 200 ms ASOI time, and compare the urea and UWS film mass accumulation at different rotating-stream tray angles, shown in Figure 22. When the angle of the rotating-stream tray increases from 20° to 30°, the accumulated urea film mass increases by 3%. When the angle of the rotating-stream tray increases from 30° to 40°, the accumulated urea film mass decreases by 5%. When the angle of the rotating-stream tray is selected as 20° or 40°, the amount of UWS wall collision is reduced, which is beneficial for reducing the risk of crystallization. Based on the results of the maximum urea film thickness and the accumulation of urea film mass, it is reasonable to choose a rotating-stream tray angle of 20° or 40°. In addition, the pressure loss and reducing agent uniformity index corresponding to the angle layout of three sets of swirl sheets were extracted. The pressure loss was 1525.9 Pa, 1305.6 Pa, 1239.8 Pa, and the reducing agent uniformity index was 95.4%, 96.3%, and 95.6%, respectively. Taking into account multiple indicators, it can be concluded that a layout with a rotating-stream tray angle of 40° is more reasonable, ensuring the minimum

risk of crystallization and pressure loss while meeting the requirements for reducing agent uniformity.

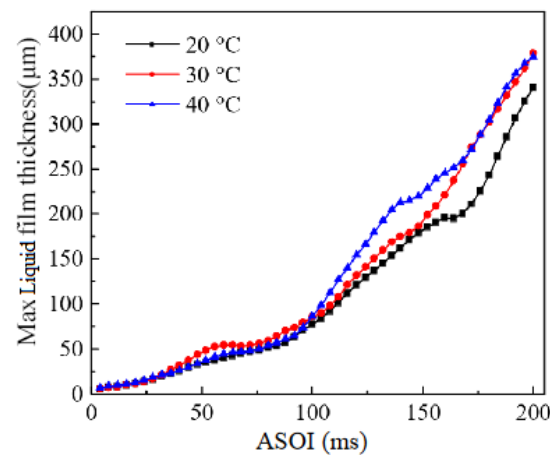


Figure 21. Variations of maximum urea film thickness with time under different rotating-stream tray angles.

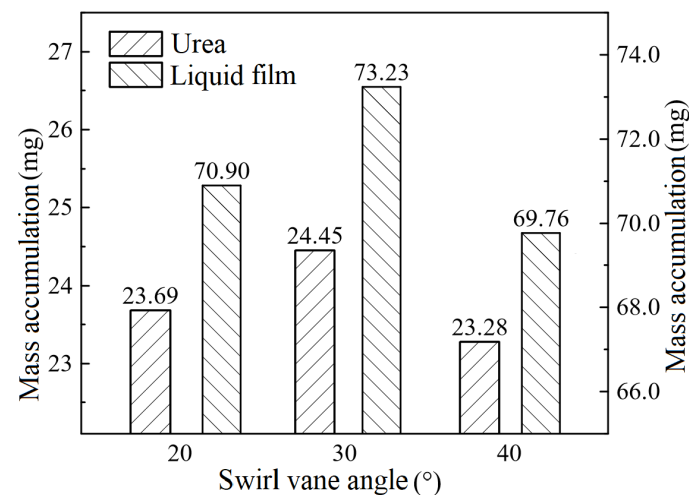


Figure 22. Variation of urea and UWS film thickness with rotating-stream tray angles.

4.2.2. Influence of the Nozzle Number on Crystallization Risk

The variation of maximum urea film thickness with time under different nozzle numbers is shown in Figure 23. The maximum urea film thickness gradually increases with the extension of spray time under all operating conditions, and the growth rate increases after 100 ms ASOI time. At a time of 200 ms ASOI, the maximum urea film thickness corresponding to different nozzle numbers is between 150 and 400 μm . After the 40 ms ASOI moment, the maximum urea film thickness corresponding to the 3-hole injector consistently exceeded that of other nozzle numbers. Within the range of 40~130 ms ASOI, the maximum urea film thickness of the 4, 5, and 6-hole injectors is basically the same. When the ASOI exceeds 130 ms, the maximum urea film thickness corresponding to the 4-hole injector begins to exceed that of the 5 and 6-hole injectors. The maximum urea film thickness corresponding to the 5- and 6-hole injectors always maintains a small gap. Overall, the nozzle number has a profound effect on the maximum urea film thickness.

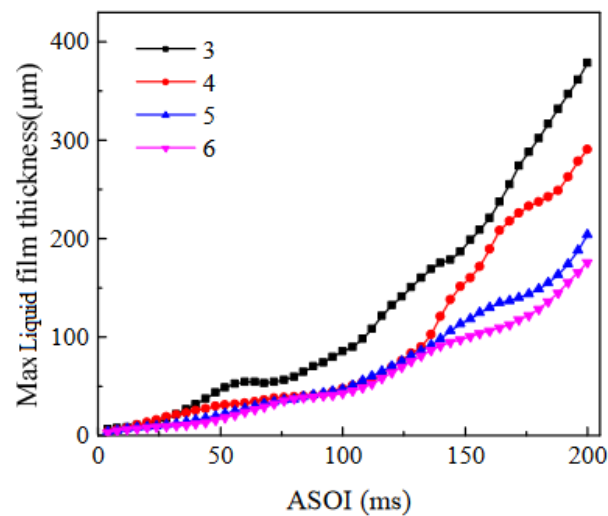


Figure 23. Variations of maximum urea film thickness with time under different nozzle numbers.

Extract urea and UWS film mass accumulation data under different nozzle numbers at 200 ms ASOI time, and compare the urea and UWS film mass accumulation under different nozzle numbers in Figure 24. The more spray holes the injector has, the more urea film mass accumulation it corresponds to. The reason is that increasing the number of orifices will increase the wall collision point of the UWS spray beam, which is conducive to the transformation of UWS droplets into urea films after they hit the wall. Similar to the situation of the maximum urea film thickness, the impact of increasing the nozzle number on the accumulation of urea film mass will gradually weaken as the nozzle number increases. For example, increasing the nozzle number from 3 to 4 increases the accumulation of urea film mass by 2%, while increasing the nozzle number from 5 to 6 increases the accumulation of urea film mass by less than 1%. Based on the impact of the nozzle number on the maximum urea film thickness and the accumulation of urea film mass, it can be concluded that increasing the nozzle number appropriately is beneficial for reducing the crystallization risk while ensuring that the atomization quality does not decrease.

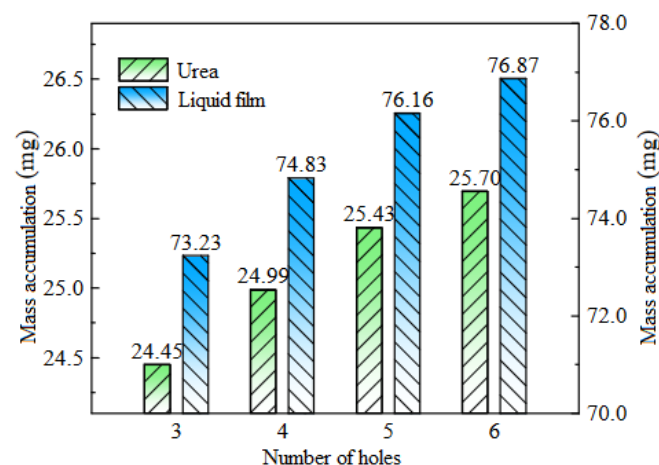


Figure 24. Accumulation of urea and UWS film under different nozzle numbers.

4.2.3. Influence of the Spray Angle on Crystallization Risk

The variation of maximum urea film thickness with time under different spray angles is shown in Figure 25. The maximum urea film thickness under different spray angles gradually increases with the extension of spray time at different growth rates. At 200 ms ASOI, the maximum urea film thickness corresponding to different spray angles is between

100 and 1000 μm . This indicates that changing the spray angle will have a profound impact on the maximum urea film thickness. If the spray angle is larger, such as 32.5° and 35.0° , the “two-stage” growth trend of the maximum urea film thickness is more obvious. Before the 100 ms ASOI moment, the difference of the maximum urea film thickness at each spray angle is inapparent. After the 100 ms ASOI moment, there began to be a significant difference in the maximum urea film thickness at each spray angle. This indicates that the impact of spray angle on urea film formation is mainly reflected in the stable development and accumulation stage of the urea film.

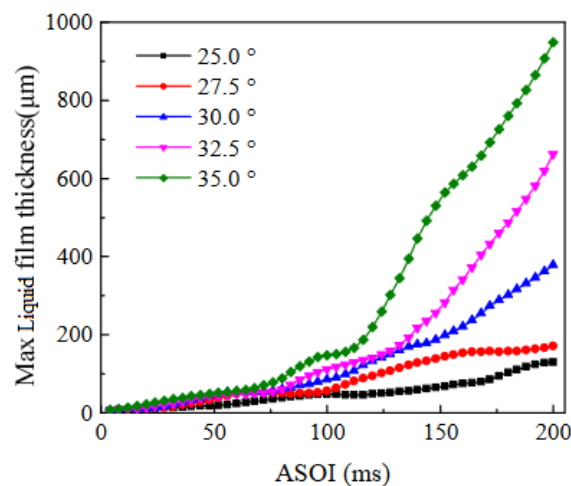


Figure 25. Variation of maximum urea film thickness with time under different spray angles.

Extract urea and UWS film mass accumulation data under different spray angles at 200 ms ASOI time, and obtain the variation of urea and UWS film mass accumulation with the spray angle, as shown in Figure 26. The accumulation of urea film mass increased at first and then decreased with the increase of spray angle. In the range of $25.0^\circ \sim 30.0^\circ$, increasing the spray angle will increase the amount of UWS hitting the wall, promote the conversion of UWS droplets into urea films, and accelerate the accumulation of urea films. Within the range of $30.0^\circ \sim 35.0^\circ$, the cumulative mass of urea film decreases with the increase of spray angle and then changes slightly. The reason is that when the spray angle increases from 32.5° to 35.0° , a portion of UWS droplet particles do not interact with the wall surface of the porous tube, but pass through the holes of the porous tube and enter the space between the swirling plate mixing tube and the porous tube, resulting in a decrease in the collision area and a decrease in the overall accumulation of urea film mass.

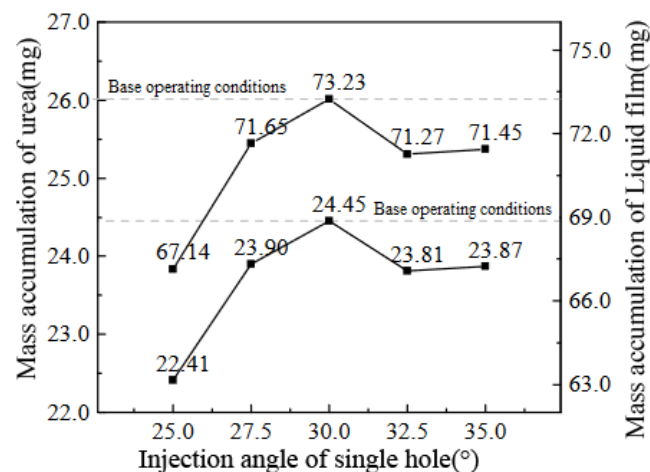


Figure 26. Changes in mass accumulation of urea and UWS film with spray angles.

The trend of the accumulation of urea film mass is different from that of the maximum urea film thickness because some droplet particles do not undergo wall collision behavior, which only affects the accumulation of urea film and does not affect the process of other droplets colliding with the wall and forming urea film accumulation at the wall collision point. Based on the variation pattern of the maximum urea film thickness and the accumulation of urea film mass, increasing the spray angle will have a significant impact on the crystallization risk, and excessive spray angles should be avoided. In addition, in terms of improving the uniformity of the reducing agent in the system, increasing the spray angle is beneficial for the diffusion distribution of UWS droplets in the film field, thereby promoting the uniform distribution of the reducing agent. Therefore, when determining the spray angle parameters, consideration should be given to the increase in crystallization risk caused by a large spray angle and the decrease in reducing agent uniformity caused by a small spray angle.

4.2.4. Influence of the Spray Cone Angle on Crystallization Characteristics

The variation of maximum urea film thickness with time under different spray cone angles is shown in Figure 27. The maximum urea film thickness under different spray cone angles gradually increases with the extension of spray time at different growth rates. At 200 ms ASOI, the maximum urea film thickness corresponding to each spray cone angle is between 200 and 400 μm , indicating that changing the cone angle of a single mist beam will have a certain impact on the maximum urea film thickness. Before the 30 ms ASOI moment, there was the inapparent difference in the maximum urea film thickness between the five groups of spray cone angles. Before the 130 ms ASOI moment, the maximum urea film thickness corresponding to a spray cone angle of 11° was basically consistent with the maximum urea film thickness corresponding to a spray cone angle of 13° . Beyond the 130 ms ASOI moment, the former always grew at a stable rate, while the latter first lagged behind the former and then approached the former at a faster rate. The variation trend of the maximum urea film thickness corresponding to a spray cone angle of 15° is similar to that at 13° . The maximum urea film thickness values fluctuate during the increase process, with only differences in the maximum urea film thickness values. The maximum urea film thickness corresponding to a spray cone angle of 17° and 19° did not show a significant difference before the 120 ms ASOI moment. After exceeding the 120 ms ASOI moment, the maximum urea film thickness of the former was relatively large, and the difference between the two remained stable.

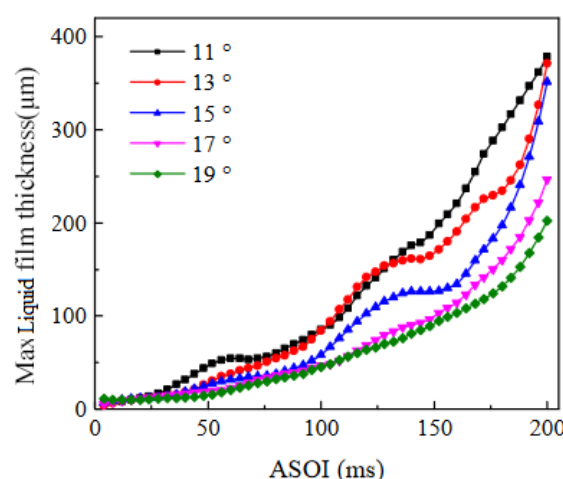


Figure 27. Variation of maximum urea film thickness with time under different spray cone angles.

Extract urea and UWS film mass accumulation data under different spray cone angles at 200 ms ASOI time, and obtain the variation of urea and UWS film mass accumulation with spray cone angles, as shown in Figure 28. The accumulation of urea film mass shows a

growth trend with the increase of the single mist beam cone angle. The reason is that while increasing the cone angle of the single mist beam, the area where urea droplets collide with the wall of the porous tube increases, resulting in more urea droplets transforming into a urea film. As the cone angle of the single mist beam increases, the variation amplitude of urea film accumulation gradually decreases. The cone angle of a single mist beam can simultaneously affect the maximum urea film thickness and urea film accumulation, and the two exhibit a “trade-off” relationship. Therefore, when determining the cone angle of the spray, a “balance” point should be found to minimize the risk of crystallization. In addition, it is also necessary to achieve collaborative control of crystallization risk by reasonably matching the parameters of spray cone angle and single hole spray angle.

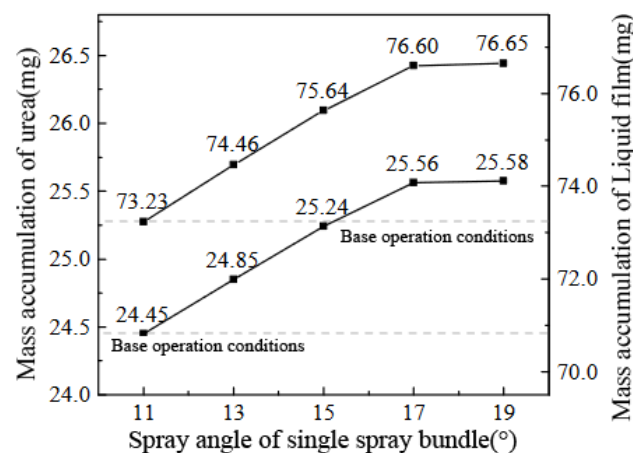


Figure 28. Changes in mass accumulation of urea and UWS film with a single spray beam cone angle.

5. Conclusions

Aiming at urea crystallization in the SCR system of diesel engines, the ammonia supply process of the SCR system is modeled in detail in this article, and a prediction model that can accurately assess the risk of urea crystallization is established by considering the processes of gas flow, heat transfer, spray atomization, component evaporation, spray wall interaction, urea film formation, and urea thermal decomposition reaction. A urea crystallization risk assessment method based on urea film thickness and urea film mass accumulation was proposed, and the feasibility of the model and assessment method was verified through bench experiments, solving the key problem of crystallization risk prediction. The main contents and conclusions of the article are as follows:

1. To ensure the efficiency of nitrogen oxide catalytic conversion under low exhaust temperature conditions and timely ammonia storage, the maximum urea film thickness method and urea film mass accumulation method are used to suppress the risk of urea crystallization.
2. Based on the established crystallization risk prediction model, the influence of exhaust temperature, exhaust flow rate, and urea spray rate on the crystallization risk of urea was deeply explored. During the process of increasing the exhaust temperature from 190 °C to 300 °C, the maximum urea film thickness decreased by 142.55 µm, and the urea film accumulation decreased by about 5%. During the process of increasing the exhaust flow rate from 60 kg/h to 300 kg/h, the maximum urea film thickness decreased to 352.77 µm but had a small impact on the urea film accumulation; after increasing the urea spray rate from a low level of 0.16 g/s to 0.32 g/s, the maximum urea film thickness increased by 428.51 µm, and when increasing from 0.24 g/s to 0.08 g/s, the urea film accumulation increased by 27%. At the same time, the urea film retention ratio was affected by exhaust temperature, exhaust flow rate, and time, and there was no positive correlation between the urea film retention ratio and urea film accumulation.

3. Considering the effects of the structure of the integrated mixer and the spray parameters on the inhibition of urea crystallization risk, the optimized scheme of using a 40° rotating-stream tray angle, a 6-hole injector, a 25° spray angle, and a 19° spray cone angle can reduce the maximum urea film thickness to 34.4% of the pre-optimization value, while slightly reducing the urea film mass accumulation, providing support for inhibiting urea crystallization risk.

Author Contributions: Conceptualization, K.S. and S.B.; methodology, K.S.; software, K.Z. and W.S.; validation, K.Z. and W.S.; formal analysis, K.Z. and G.Z.; investigation, K.S., K.Z. and G.Z.; resources, S.B. and C.L.; data curation, K.S. and G.Z.; writing—original draft preparation, K.S., K.Z., and W.S.; writing—review and editing, K.Z., G.Z., W.S., and H.C.; visualization, G.Z. and K.Z.; supervision, G.L., S.B., and C.L.; project administration, K.S.; funding acquisition, G.L. and S.B. All authors have read and agreed to the published version of the manuscript.

Funding: This work was funded by the Construction Machinery Intelligent Equipment Innovation and Entrepreneurship Community of Shandong, China (grant number GTT2021105), Department of Science & Technology of Shandong Province, China (grant number 2021TSGC1334), Asset & Laboratory Management Department of Shandong University, China (grant number sy20232305), and the Undergraduate School of Shandong University, China (grant number 2022Y155).

Institutional Review Board Statement: Institutional review is not applicable, as the paper did not involve humans or animals.

Informed Consent Statement: Informed consent is not applicable, as the paper did not involve humans.

Data Availability Statement: The data presented in this study are available in the article.

Acknowledgments: I personally appreciate the editors and reviewers for their constructive and detailed critiques that contributed to the quality of this paper.

Conflicts of Interest: The authors declare no conflicts of interest.

References

1. Johnson, T.; Joshi, A. Review of Vehicle Engine Efficiency and Emissions. In Proceedings of the WCX™ 17: SAE World Congress Experience, Detroit, MI, USA, 4–6 April 2017. [\[CrossRef\]](#)
2. Castro, N.; Toledo, M.; Amador, G. An Experimental Investigation of the Performance and Emissions of a Hydrogen-Diesel Dual Fuel Compression Ignition Internal Combustion Engine. *Appl. Therm. Eng.* **2019**, *156*, 660–667. [\[CrossRef\]](#)
3. Koten, H. Hydrogen effects on the diesel engine performance and emissions. *Int. J. Hydrogen Energy* **2018**, *43*, 10511–10519. [\[CrossRef\]](#)
4. Zixian, Z.; Chaofeng, S.; Jue, C. Effects of Private Electric Vehicles on Carbon Emission Reduction in China during Whole Life Cycle. *Res. Environ. Sci.* **2021**, *34*, 2076–2085.
5. Li, Y.; Ha, N.; Li, T. Research on Carbon Emissions of Electric Vehicles throughout the Life Cycle Assessment Taking into Vehicle Weight and Grid Mix Composition. *Energies* **2019**, *12*, 3612. [\[CrossRef\]](#)
6. Leach, F.; Kalghatgi, G.; Stone, R.; Miles, P. The scope for improving the efficiency and environmental impact of internal combustion engines. *Transp. Eng.* **2020**, *1*, 100005. [\[CrossRef\]](#)
7. Yusuf, A.A.; Inambao, F.L.; Ampah, J.D. Evaluation of biodiesel on speciated PM_{2.5}, organic compound, ultrafine particle and gaseous emissions from a low-speed EPA Tier II marine diesel engine coupled with DPF, DEP and SCR filter at various loads. *Energy* **2022**, *239*, 121837. [\[CrossRef\]](#)
8. Yusuf, A.A.; Yusuf, D.A.; Jie, Z.; Bello, T.Y.; Tambaya, M.; Abdullahi, B.; Muhammed-Dabo, I.A.; Yahuza, I.; Dandakouta, H. Influence of waste oil-biodiesel on toxic pollutants from marine engine coupled with emission reduction measures at various loads. *Atmos. Pollut. Res.* **2022**, *13*, 101258. [\[CrossRef\]](#)
9. Smith, H.; Lauer, T.; Mayer, M.; Pierson, S. Optical and Numerical Investigations on the Mechanisms of Deposit Formation in SCR Systems. *SAE Int. J. Fuels Lubr.* **2014**, *7*, 525–542. [\[CrossRef\]](#)
10. Smith, H.; Zöchbauer, M.; Lauer, T. Advanced Spray Impingement Modelling for an Improved Prediction Accuracy of the Ammonia Homogenisation in SCR Systems. In Proceedings of the SAE 2015 World Congress & Exhibition, Detroit, MI, USA, 21–23 April 2015. [\[CrossRef\]](#)
11. Huang, Z.; Yin, K.; Zhou, Z.; Wang, Z.; Yang, W.; Zhou, J. Experimental investigation on evaporation characteristics of urea-aqueous-solution droplet. *Chem. Ind. Eng. Prog.* **2014**, *33*, 817–823.
12. Bernhard, A.M.; Czekaj, I.; Elsener, M.; Wokaun, A.; Kröcher, O. Evaporation of Urea at Atmospheric Pressure. *J. Phys. Chem. A* **2011**, *115*, 2581–2589. [\[CrossRef\]](#) [\[PubMed\]](#)

13. Lundström, A.; Snelling, T.; Morsing, P.; Gabrielsson, P.; Senar, E.; Olsson, L. Urea decomposition and HNCO hydrolysis studied over titanium dioxide, Fe-Beta and γ -Alumina. *Appl. Catal. B Environ.* **2011**, *106*, 273–279. [\[CrossRef\]](#)
14. Bai, C.; Gosman, A.D. Development of Methodology for Spray Impingement Simulation. In Proceedings of the International Congress & Exposition, Detroit, MI, USA, 27 February–2 March 1995. [\[CrossRef\]](#)
15. Kuhnke, D. Spray Wall Interaction Modelling by Dimensionless Data Analysis. Ph.D. Thesis, Technische Universität Darmstadt, Aachen, Germany, 2004.
16. Strots, V.O.; Santhanam, S.; Adelman, B.J.; Griffin, G.A.; Derybowski, E.M. Deposit Formation in Urea-SCR Systems. *SAE Int. J. Fuels Lubr.* **2009**, *2*, 283–289. [\[CrossRef\]](#)
17. Ebrahimi, V.; Nicolle, A.; Habchi, C. Detailed modeling of the evaporation and thermal decomposition of urea-water solution in SCR systems. *AIChE J.* **2012**, *58*, 1998–2009. [\[CrossRef\]](#)
18. Jain, A.; Barman, J.; Patchappalam, K.; Gedela, S. A Study on the Factors Affecting the Formation of Urea Crystals and Its Mitigation for SCR After-Treatment Systems. In Proceedings of the Symposium on International Automotive Technology 2017, Pune, India, 18–21 January 2017. [\[CrossRef\]](#)
19. Sadashiva, P.S.; Natesan, K.; Nayak, N.S. Effects of thermal treatments on characteristics and morphological variations in the deposits of urea-SCR systems. *Environ. Sci. Pollut. Res.* **2021**, *28*, 56711–56726. [\[CrossRef\]](#)
20. Stiesch, G. *Modeling Engine Spray and Combustion Processes*; Springer: Berlin/Heidelberg, Germany, 2003. [\[CrossRef\]](#)
21. Gan, X. Foundmental Research on Reducing Agent Adding Process of Urea-SCR Systems for Diesel Engines. Ph.D. Thesis, Zhejiang University, Hangzhou, China, 2017.
22. Tang, T.; Yao, D.; Wu, F.; Liu, Z.; Hu, A.; He, H. Simulation of Urea Addition Based on Detailed Evaporation and Thermolysis for Urea-SCR. *Trans. CSICE* **2020**, *38*, 538–544. [\[CrossRef\]](#)
23. Yim, S.D.; Kim, S.; Baik, J.; Nam, I.S.; Mok, Y.S.; Lee, J.H.; Cho, B.; Oh, S. Decomposition of urea into NH₃ for the SCR process. *Ind. Eng. Chem. Res.* **2004**, *43*, 4856–4863. [\[CrossRef\]](#)
24. Brack, W.; Heine, B.; Birkhold, F.; Kruse, M.; Schoch, G.; Tischer, S.; Deutschmann, O. Kinetic modeling of urea decomposition based on systematic thermogravimetric analyses of urea and its most important by-products. *Chem. Eng. Sci.* **2014**, *106*, 1–8. [\[CrossRef\]](#)
25. Leilei, D.; Chunlan, M.; Yitao, M.; Wenjun, H.; Hualin, L. Detailed Chemical Reaction Mechanism Model of SCR Urea Decomposition for Diesel Engine. *Veh. Engine* **2019**, 28–34. [\[CrossRef\]](#)
26. Junbo, Y.; Chunlan, M.; Wenjun, H.; Leilei, D.; Hualin, L.; Yitao, M. Detailed Reaction Pathways of Urea Deposit in Diesel Engine with Selective Catalytic Reduction System. *Trans. CSICE* **2020**, *38*, 9.

Disclaimer/Publisher’s Note: The statements, opinions and data contained in all publications are solely those of the individual author(s) and contributor(s) and not of MDPI and/or the editor(s). MDPI and/or the editor(s) disclaim responsibility for any injury to people or property resulting from any ideas, methods, instructions or products referred to in the content.